Chapter 12
Targeting Carbonic Anhydrase IX in Tumor Imaging and Theranostic Cancer Therapy

Joseph Lau, Kuo-Shyan Lin, and François Bénard

Abstract Carbonic anhydrase IX (CA-IX) is an endogenous marker for hypoxia and is regulated by the von Hippel-Lindau/hypoxia-inducible factor (VHL/HIF) oxygen-sensing pathway. CA-IX is overexpressed in many solid malignancies where aberrant vasculature and limited perfusion create low oxygen niches within the tumor microenvironment. Dysregulation of the VHL/HIF signaling pathway can lead to constitutive expression of CA-IX—a phenotype associated with clear cell renal cell carcinomas (ccRCCs). As a cell-surface metalloenzyme, CA-IX works in tandem with other proteins to regulate intracellular pH in response to hypoxia-induced metabolism. In recent years, there has been evidence implicating CA-IX in potentiating cancer invasion and metastasis. Accordingly, the inhibition of CA-IX catalytic activity represents an attractive option for the management of ccRCC and other solid tumors. In this chapter, we discuss the development of CA-IX radiopharmaceuticals and their roles in delineating tumoral CA-IX expression through imaging in preclinical and clinical settings. We will also review agents that have been repositioned as endoradiotherapeutic agents for theranostic application.

Keywords Carbonic anhydrase IX · Hypoxia · Microenvironment · Imaging · Therapy · ccRCC

J. Lau · K.-S. Lin · F. Bénard (✉)
Department of Molecular Oncology, BC Cancer Agency, Vancouver, BC V5Z 1L3, Canada
e-mail: fbenard@bccrc.ca

J. Lau
e-mail: jlau@bccrc.ca

K.-S. Lin
e-mail: klin@bccrc.ca

12.1 Introduction

Tumor hypoxia, a salient feature of solid tumors, is a negative prognostic marker for many cancers (Harris 2002; Walsh et al. 2014). Low oxygen availability depresses the efficacy of conventional radiation therapy and chemotherapy (Harris 2002; Walsh et al. 2014). Moreover, a hypoxic tumor microenvironment exerts selection pressure for resistant and aggressive clonal populations, increasing the predisposition for metastasis (Wilson and Hay 2011). Hypoxia-activated prodrugs, tumor vasculature remodeling agents, and modulators of hypoxia-induced metabolism are attractive anti-cancer agents (Wilson and Hay 2011). Carbonic anhydrase IX (CA-IX) is a biomarker for tumor hypoxia and a promising target for treating solid malignancies (Supuran 2008; McDonald et al. 2012). CA-IX regulates intracellular pH and mediates survival under hypoxic conditions. CA-IX acidifies the tumor microenvironment and primes it for invasion and distant metastasis (McDonald et al. 2012). The pharmaceutical inhibition of CA-IX activity by small molecule pharmaceuticals is being investigated in clinical trials (Supuran 2017). The success of these agents will depend on appropriate patient stratification.

Single photon emission computed tomography (SPECT) and positron emission tomography (PET) represent nuclear imaging modalities that can quantify drug-target expression in primary and metastatic lesions to predict drug sensitivity to hypoxia-based treatments (Weissleder and Mahmood 2001; Jadvar et al. 2018). In addition to identifying potential responders, SPECT and PET can be used to assess pharmacokinetic parameters and drug-target engagement, and to monitor treatment responses in a non-invasive manner (Weissleder and Mahmood 2001; Jadvar et al. 2018). Some imaging radiopharmaceuticals used to target CA-IX have been converted to endoradiotherapeutic agents. In this chapter, we will discuss the suitability of CA-IX as a druggable biomarker underpinning tumor hypoxia. We will review the development of CA-IX radiopharmaceutical agents (antibodies, peptides, and small molecules) in clinical and preclinical settings. Finally, we offer our perspectives for the translation and integration of these radiopharmaceuticals in nuclear medicine.

12.2 Targeting CA-IX as a Biomarker of Tumor Hypoxia

Cancer cells in solid tumors are constantly exposed to fluctuating oxygen levels within the tumor microenvironment. The process of developing hypoxia is independent of a tumor's size, stage, grade, or histology (Bennewith and Dedhar 2011). When oxygen tension is low (pO_2 value < 10 mmHg), most cancer cells undergo metabolic reprogramming regulated by the von Hippel-Lindau/hypoxia-inducible factor (VHL/HIF) oxygen-sensing pathway (Bennewith and Dedhar 2011; Parks et al. 2011). HIF-activated cancer cells reduce their reliance on oxidative phosphorylation, and instead shift to glycolysis to produce adenosine triphosphate (ATP) (Parks et al. 2011). Glycolysis provides the requisite ATP and biosynthetic building

blocks for survival, but concurrently lowers intracellular pH (pH_i) (Parks et al. 2011). In response to this new stressor, cancer cells overexpress CA-IX to modulate pH_i. CA-IX is a member of the carbonic anhydrase α-family (Alterio et al. 2012; Wykoff et al. 2000). As a zinc metalloenzyme, CA-IX catalyzes the interconversion of water and carbon dioxide to bicarbonate and hydrogen ions ($H_2O + CO_2 \leftrightarrow HCO_3^- + H^+$) (Hilvo et al. 2008). The HCO_3^- ions enter the cell through transporter systems to re-establish an alkaline pH_i. The H^+ ions from the reaction go on to acidify the tumor microenvironment, promoting invasion and metastasis. Researchers often measure pH change in culture medium as a means to assay CA-IX catalytic activity in cancer cell lines (Lou et al. 2011).

CA-IX is the most upregulated protein in response to HIF-1α activation; thus, it is a well-regarded endogenous marker of cellular hypoxia (Wykoff et al. 2000). While most biomarkers in oncology are specific to cancer subtypes, CA-IX overexpression is broadly observed in solid malignancies including but not limited to head and neck, breast, lung, ovarian, and renal cancers (McDonald et al. 2012). In normal tissues, CA-IX expression is restricted to the small intestine, pancreas, and male efferent epithelial ducts (McDonald et al. 2012). The differential expression of CA-IX in cancer and normal tissues allows for adequate signal-to-noise ratios and therapeutic indices for imaging and treatment, respectively. The stability of CA-IX, its accessibility as a cell-surface protein, and the plethora of potent binders are additional merits that support CA-IX targeting strategies.

It is imperative for researchers to understand that there are situations where CA-IX expression does not correlate with the oxygen level within a tumor. Discordant CA-IX and HIF-1α expression levels have previously been reported in vivo (Li et al. 2015). In transient hypoxia, leveraging CA-IX expression to interpolate tumor hypoxia may lead to overestimation of the hypoxic subvolume. This observation was attributed to the disparate biological half-lives in re-oxygenated cells (hours for CA-IX and minutes for HIF-1α) (Rafajová et al. 2004; Moroz et al. 2009). As communicated by Kulaz et al., the expression of CA-IX correlates better with the transcriptional activity of HIF-1α rather than HIF-1α expression (Kaluz et al. 2009). At the other extreme, there are instances where CA-IX expression is conspicuously absent in hypoxic conditions. Loss-of-function mutations in HIF-1α have been observed in cell lines (Morris et al. 2009), and there are cancers that preferentially express HIF-2α and HIF-2α-regulated genes in response to hypoxia (Li et al. 2009; Holmquist-Mengelbier et al. 2006).

12.3 Methods for Detecting Tumor Hypoxia

The polarographic electrode is the current gold standard for determining oxygenation levels in live tissues (Walsh et al. 2014). The methodology requires the insertion of electrodes in superficial/accessible tumors. It is limited by sampling bias and an inability to differentiate between hypoxia and necrosis. Given the extensive role of PET imaging in diagnosis, staging, and disease monitoring, an area of active research

has been the development of hypoxia imaging agents (Lopci et al. 2014; Fleming et al. 2015). FMISO, FAZA, EF5, and HX4 are examples of radio-fluorinated nitroimidazole derivatives being evaluated in the clinic. Following passive diffusion into cells, these agents are reduced by one-electron-transfer reactions to form reactive intermediates. In a normoxic cell, the nitro-radical anions undergo oxidation to reform the parent compounds, which then permeate out of the cell. In a hypoxic cell, the nitro-radical anions undergo additional reduction and bind to macromolecules. The binding to proteins or nucleic acids 'traps' the radioactivity inside hypoxic cells. FMISO is the most heavily investigated nitroimidazole in the clinic (Rajendran and Krohn 2015). However, the routine clinical use of FMISO and other derivatives is hampered by their slow clearance from normal tissues. Because of pharmacokinetics and mechanism of uptake, image acquisition is performed several hours post-injection (p.i.) and typically results in low-contrasted images. The hypoxia cut-off value for FMISO is institution- and scanner-dependent. For instance, Rajendran and colleagues set a tumor-to-background ratio of ≥ 1.2 at 2 h p.i. to delineate hypoxic tumors for sarcoma patients (Rajendran et al. 2003). The need to identify radiopharmaceuticals with higher sensitivity and faster pharmacokinetic has put a focus on targets like CA-IX.

12.4   CA-IX Expression in Clear Cell Renal Cell Carcinoma

The development of CA-IX radiopharmaceuticals is also prompted by the pathophysiology of clear cell renal cell carcinomas (ccRCCs), a subtype that comprises approximately 75% of all renal cell carcinomas (Hsieh et al. 2017). It is estimated that up to 92% of ccRCCs harbor genetic or epigenetic abnormalities that lead to the inactivation of the von Hippel-Lindau (VHL) tumor suppressor gene (Clark 2009; Zhang and Zhang 2018). VHL is a negative regulator and a binding partner of HIF-1α. Under normoxic conditions, VHL binds to HIF-1α to form a complex that is poly-ubiquitinated and targeted for proteasomal degradation (Pastorekova et al. 2008). This process inhibits HIF-1α activation and CA-IX transcription (Pastorekova et al. 2008). The dysregulation of VHL/HIF-1α pathway induces the constitutive expression of CA-IX, making it a rational target for ccRCC (Fig. 12.1).

When ccRCC is localized and treatable with surgery, the five-year survival rate for ccRCC is favorable at 91.7% (Ridge et al. 2014). However, diagnosis for ccRCC is not trivial with most cases being discovered as incidental findings (Gorin et al. 2015). Most anatomical imaging modalities are unable to differentiate between malignant and benign lesions as well as histological subtypes (Gorin et al. 2015). PET imaging with ^{18}F-FDG is better-suited for metastatic disease than primary lesion detection due to the renal excretion of imaging agent (Gorin et al. 2015; Escudier et al. 2016). A substantial portion of patients with benign masses, approximately 20%, receive surgical intervention when active monitoring would suffice (Gorin et al. 2015). CA-IX imaging enables radiologists and oncologists to accurately diagnose ccRCC and provide standard of care. Patients with late stage metastatic disease have
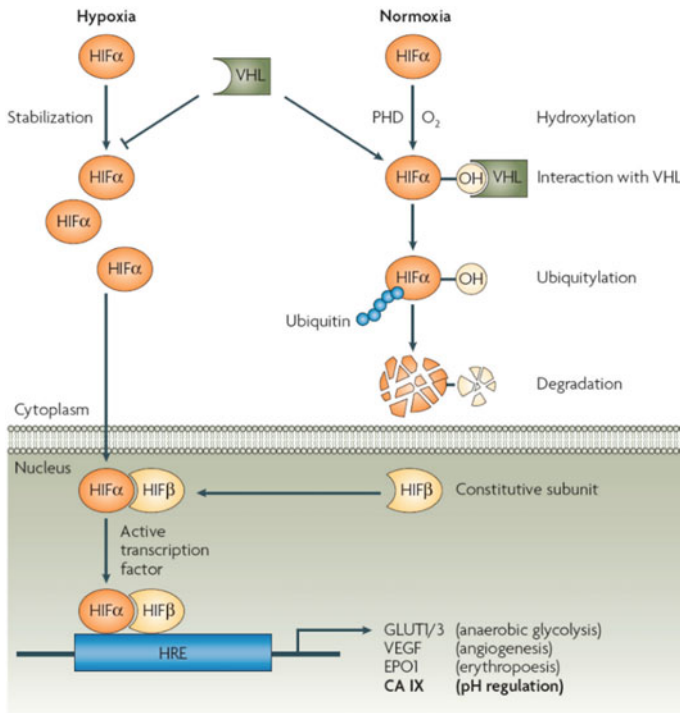
Fig. 12.1 Functional activity of HIF-1α and its regulation by oxygen. In normoxia, HIF-1α is post-translationally modified by proline hydroxylases (PHDs). These enzymes use oxygen as a substrate and Fe(II) and 2-oxoglutarate (2-OG) as cofactors. When HIF-1α is hydroxylated by PHDs, it binds with the VHL tumor suppressor protein. The VHL/HIF-1α complex becomes rapidly ubiquitinated and degraded. In hypoxia, HIF-1α escapes hydroxylation and VHL binding, accumulates in cytoplasm, translocates to the nucleus, and dimerizes with HIF-1β. HIF-1α/β binds to hypoxia-response elements (HREs) in the promoter region of the target genes like CA-IX, recruits transcriptional co-activators to initiate transcription. Figure adapted with permission from Supuran (2012) in accordance with the Creative Commons Attribution (CC BY-NC 4.0) license

few available treatments. Currently, first-line therapy for metastatic ccRCC consists of targeted therapies against rapamycin and the vascular epidermal growth factor receptor (Hsieh et al. 2017). Unfortunately, the five-year survival rate for ccRCC patients with distant metastasis is dismal at 12.3% (Ridge et al. 2014). The poor prognosis for metastatic ccRCC is the major impetus for developing CA-IX-targeted treatments like radioimmunotherapy (RIT).

12.5 Monoclonal Antibodies

Monoclonal antibodies (mAbs) are a class of biologics that are used in targeted therapies. Known for their stability, binding affinity, and target selectivity, mAbs can abrogate cell-signaling, inhibit angiogenesis, regulate osteoclast function, or modulate immune response (Chiavenna et al. 2017). mAbs can also recruit immune cells to activate antibody-dependent cell-mediated cytotoxicity, complement-dependent cytotoxicity, or antibody-dependent cell phagocytosis (Scott et al. 2012). Finally, they can be modified to selectively deliver cytotoxic drugs or ionizing radiation (Sharkey and Goldenberg 2009).

Many mAbs have been developed for CA-IX targeting (Chrastina et al. 2003; Čepa et al. 2018; Ahlskog et al. 2009), but girentuximab (cG250) remains the most clinically investigated agent (Oosterwijk-Wakka et al. 2013). The first generation of cG250 was isolated as murine G250 by Oosterwijk et al. by hybridoma screening after immunizing mouse splenocytes with renal cancer homogenates (Oosterwdk et al. 1986). The proteoglycan (PG)-like domain of CA-IX is the epitope site for cG250. This domain is exclusive to CA-IX compared to other members of the CA family (McDonald et al. 2012). cG250 can induce antibody-dependent cellular cytotoxicity (Oosterwijk-Wakka et al. 2013). In a phase III study, cG250 was evaluated as an adjuvant monotherapy in patients with localized high-risk ccRCC after nephrectomy (Chamie et al. 2017). Patients treated with cG250 did not show improvement for disease-free survival (DFS) and overall survival (OS). Patients whose tumors showed higher DFS, but this was not statistically significant compared to placebo. Histology scoring was obtained by multiplying intensity of staining (1–3) by percent of positive cells (0–100) to yield a range of 0 to 300. In the subsequent section, we will review radiolabeled derivatives of cG250 for theranostic applications (Table 12.1).

12.5.1 Imaging with G250/cG250

The first clinical study with radiolabeled G250 (^{131}I-mAbG250) was conducted by Oosterwijk et al. at the Ludwig Institute for Cancer Research (Oosterwijk et al. 1993). The primary objective of this phase I study was to assess safety and biodistribution of ^{131}I-mAbG250. Sixteen patients suspected of having RCC received ^{131}I-mAbG250 intravenously 7 or 8 d before scheduled nephrectomy. Twelve patients had positive scans from whole-body planar imaging at 3 d p.i. Histology of the biopsied tissues showed that 11 patients had ccRCC and 1 patient had RCC of the granular subtype. CA-IX expression in the scan-positive lesions ranged from <5% to 100% based on immunohistochemistry. For the 4 negative scans, 3 patients had RCC of the granular or spindle subtype and 1 patient had a benign mass. ^{131}I-mAbG250 was well-tolerated in patients and accumulated specifically in CA-IX expressing lesions.

[131]I-cG250 was used as part of RIT protocols to identify responders and monitor treatment response; however, the high energy gamma emissions of ^{131}I and reliance

Table 12.1 Clinical studies with radiolabeled G250/cG250 for imaging or therapy. Adapted from Lau et al. (2017) in accordance with the Creative Commons Attribution (CC BY-NC 4.0) license

Imaging

Agent	# Patients enrolled[a]	Indication	Detection	Sensitivity and selectivity	Clinical stage	Refs.
[131]I-mAbG250	16	Primary RCC	11/11 ccRCC pts	NR	Phase I dose escalation	Oosterwijk et al. (1993)
[124]I-cG250	26(25)	Primary RCC	15/16 ccRCC pts	94 and 100%	Phase I single dose	Divgi et al. (2007)
[124]I-cG250	226(195)	Primary RCC	124/143 ccRCC pts	86 and 76%	Phase III	Divgi et al. (2013)
[111]In-cG250 ^{131}I-cG250	5	Metastatic ccRCC	47 lesions 30 lesions	NR	Phase I/II intrapatient comparison	Brouwers et al. (2003)
[111]In-cG250	29(22)	Metastatic ccRCC	15/15 ccRCC pts	NR	Partly retrospective	Muselaers et al. (2013)
[89]Zr-cG250	30(29)	RCC/ ccRCC	18/19 ccRCC pts	NR	Phase I/II	Hekman et al. (2018a)

Therapy

Agent	# Patients enrolled[a]	Indication	Response	Duration of response	Clinical stage	Refs.
[131]I-mAbG250	33	Metastatic ccRCC	17 SD	2–3 mo	Phase I/II dose escalation	Divgi et al. (1998)
			16 PD			
[131]I-cG250	12(8)	Metastatic ccRCC	1 PR	9 + mo	Phase I dose escalation	Steffens et al. (1999)
			1 SD	3–6 mo		
			6 PD			
[131]I-cG250	15(14)	Metastatic ccRCC	7 SD	4–13 mo	Phase I dose fractionation	Divgi et al. (2004)
			7 PD			
[131]I-cG250	29(15)	Metastatic ccRCC	5 SD	3–12 mo	Phase I/II two doses	Brouwers et al. (2005)
			10 PD			
[177]Lu-cG250	23	Metastatic ccRCC	1 PR	9 + mo	Phase I dose escalation	Stillebroer et al. (2013)
			12 SD	3 + mo		
			10 PD			
[177]Lu-cG250	16(14)	Metastatic ccRCC	1 PR	NR	Phase II	Muselaers et al. (2016)
			7 SD;	3 + mo		
			6 PD			

[a]Number in bracket represents the number of patients that satisfied evaluation criteria G250: murine monoclonal G250 antibody; cG250: chimeric monoclonal G250 antibody; ccRCC: clear cell renal cell carcinoma; RCC: renal cell carcinoma; SD: stable disease; PD: progressive disease; PR: partial response; pts: patients; NR: not reported

on collimators for detection are not ideal for image quantification (Rault et al. 2007). Subsequently, another iodine isotope [124]I was used to radiolabel cG250 (Divgi et al. 2007). [124]I-cG250 uses PET imaging, a modality that uses coincidence detection for enhanced sensitivity and resolution. Divgi et al. evaluated [124]I-cG250 in a phase I study for preoperative characterization of RCC with indeterminate masses (Divgi et al. 2007). Twenty-six patients received an imaging dose of 185 MBq/10 mg 1 wk prior to surgery. PET/CT imaging was performed within 3 h prior to surgery. When the tumor-to-kidney (T:K) ratio was >3, the scan was designated as positive. Sixteen cases of ccRCC were confirmed by histology and 15 of those had positive PET scans. Patients ($n = 9$) who had a negative PET scan did not have ccRCC. One patient was excluded from analysis because of an immunologically inactive infusion of [124]I-cG250. Overall, the sensitivity and specificity of [124]I-cG250 were 94% and 100%.

[124]I-cG250 advanced to a phase III study, where its average sensitivity and selectivity for ccRCC was compared with contrast-enhanced CT (CECT) (Divgi et al. 2013). In total, 226 patients were enrolled, and 195 patients were assessable. Patients received 185 MBq/13.7 mg [124]I-cG250, and PET/CT acquisitions were performed 2-6 d following administration. CECTs were performed within 48 h of the PET/CT session. [124]I-cG250 showed better average sensitivity (86% vs. 76%) and selectivity (76% vs. 47%) than CECT for differentiating ccRCC from non-ccRCC. Positive predictive value (PPV), negative predictive value (NPV), and accuracy were calculated as secondary efficacy variables. [124]I-cG250 had an accuracy value of 86%, a PPV of 94%, and an NPV 69%. The results suggest that [124]I-cG250 PET can guide management and surgical decisions for patients with indiscriminate renal lesions. A secondary phase III study was recommended by the Food and Drug Administration, but commercial development appears stalled. Potential limitations for the clinical adoption of [124]I-cG250 include high cost of [124]I production, and in vivo dehalogenation.

One of the first radiolabels used for SPECT imaging with cG250 was indium-111 (^{111}In). cG250 was conjugated with the bifunctional chelators 1,4,7,10-tetraazacyclododecane-1,4,7,10-tetraacetic acid (DOTA) or diethylenetriaminepentaacetic acid (DTPA) for ^{111}In-labeling. ^{111}In-DOTA-cG250 was used as a companion imaging agent for ^{177}Lu-DOTA-cG250 RIT studies. Five ccRCC patients that were part of a phase I/II RIT study with ^{131}I-cG250 were recruited for an intrapatient comparison of ^{111}In-DTPA-cG250 versus ^{131}I-cG250 scintigraphy (Brouwers et al. 2003). ^{111}In-DTPA-cG250 enabled the visualization of more metastatic lesions than ^{131}I-cG250 at 4 d p.i. ($n = 47$ vs. $n = 30$). Radioactivity accumulation in 25 lesions were quantified; ^{111}In-DTPA-cG250 had higher uptake in 20 lesions and yielded better tumor-to-blood ratios. In a subsequent study, ^{111}In-DTPA-cG250 was evaluated in a cohort of 29 patients, of which 22 presented with a renal mass (Muselaers et al. 2013). Some of the patients were part of a secondary imaging study in which the effect of sorafenib on ^{111}In-DTPA-cG250 was studied. ^{111}In-DTPA-cG250 showed uptake in 16 patients, with 15 cases confirmed to be ccRCC by histopathology. The remaining patient had a type 2 papillary RCC that was also CA-IX positive.
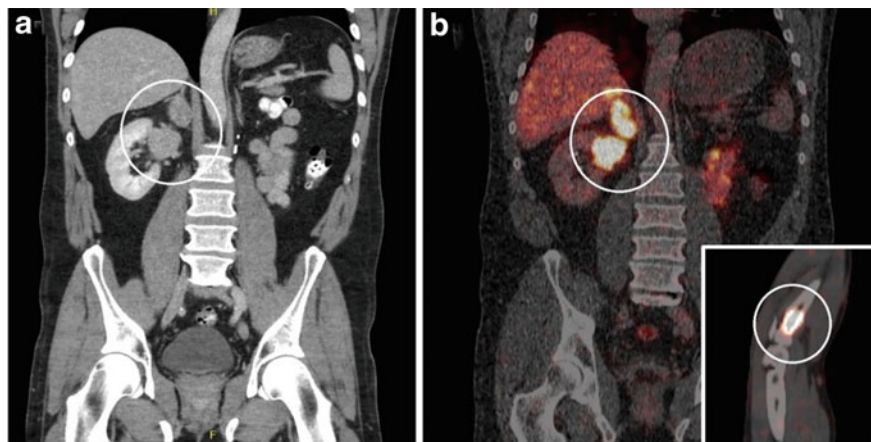
Fig. 12.2 ^{89}Zr-cG250 imaging in a patient who previously underwent a radical nephrectomy but presented with (**a**) a new renal tumor and a solitary adrenal metastasis on CT. (**b**) Uptake of ^{89}Zr-cG250 was observed in the primary renal mass, the adrenal lesion, and a previously unidentified lesion in the proximal radius. Patient had surgery and also radiotherapy for the bone lesion. Of note, the proximal radius was not in the field of view of the initial conventional imaging (CT-thorax/abdomen). Figure adapted with permission from Hekman et al. (2018a)

Recently, Hekman et al. reported the evaluation of ^{89}Zr-cG250 in a phase I/II study (Fig. 12.2) (Hekman et al. 2018a). Thirty patients suspected with ccRCC were recruited for the study and divided into two groups. The first group consisted of 16 patients with an indistinct renal mass, while the second group consisted of 14 patients with suspected recurrent/metastatic ccRCC. For the first group, six patients had a positive PET scan. Five of the 6 underwent surgery confirming ccRCC, and the patient with VHL syndrome had additional positive lesions and underwent cyroablation for debulking. One patient had two lesions, one positive and one negative on PET, but was not treated due to complex surgical history. Nine patients with negative PET scans were followed by active surveillance; none progressed within the follow-up period (13 ± 4.9 mo). In the second group, ^{89}Zr-cG250 was used to determine treatment intent. A change in clinical management occurred for 5 patients, with 3 patients avoiding biopsies due to positive PET scans. The decisions to change management was not solely dependent on ^{89}Zr-cG250-PET but included consideration of other clinical parameters.

As demonstrated through these studies, mAbs are powerful targeting vectors for imaging applications. The prolonged residence time of mAbs in blood allows for increased exposure to the target of interest, facilitating more binding events and increasing tumor uptake. However, the slow pharmacokinetics of mAbs often necessitates a clearance period of several days before optimal imaging contrast can be achieved. Antibody fragments generated from enzymatic cleavage by papain or pepsin maintain affinity for their target of interest but are structurally smaller (~55 and 110 kDa for Fab and F(ab')$_2$) (Sharkey and Goldenberg 2009; Freise and Wu

2015). The removal of the fragment crystallizable region reduces the likelihood of immunogenicity. Using these fragments as imaging agents would reduce radiation exposure and enable same-day imaging, providing logistical and clinical advantages. Predictably, cG250 antibody fragments, cG250-Fab, and cG250-F(ab')$_2$, have been investigated as imaging agents.

Carlin et al. compared the uptake of ^{111}In-DOTA-cG250, ^{111}In-DOTA-F(ab')$_2$-cG250, and ^{111}In-DOTA-Fab-cG250 in athymic mice bearing HT-29 human colorectal cancer xenografts (Carlin et al. 2010). This tumor model is considered a hypoxic cancer model. Biodistribution studies were performed at 2, 4, and 7 d p.i. for ^{111}In-DOTA-cG250, and at 6 and 24 h p.i. for ^{111}In-DOTA-F(ab')$_2$-cG250 and ^{111}In-DOTA-Fab-cG250. The harvested tumors were fluorescently stained for CA-IX, hypoxia (pimonidazole), and blood perfusion (Hoechst). The tumor uptake of ^{111}In-DOTA-cG250 at 7 d p.i. was 26.4 $\pm$ 5.7%ID/g, which corresponded to tumor-to-blood (T:B) and tumor-to-muscle (T:M) ratios of 6.6 and 69. ^{111}In-DOTA-F(ab')$_2$-cG250 and ^{111}In-DOTA-Fab-cG250 showed focal but lower uptake (9.3 $\pm$ 2.1%ID/g and 3.5 $\pm$ 1.7%ID/g at 24 h p.i.), and lower T:B (4.6 and 16.6) and T:M ratios (8.9 and 6.7). ^{111}In-DOTA-F(ab')$_2$-cG250 and ^{111}In-DOTA-Fab-cG250 are capable of targeting CA-IX in hypoxic niches with a shorter distribution phase, but this comes at the expense of absolute uptake and contrast ratios.

Hoeben et al. used ^{89}Zr-cG250-F(ab')$_2$ for imaging hypoxia-mediated CA-IX expression in the SCCNij3 human head and neck squamous cell carcinoma model (Hoeben et al. 2010). ^{89}Zr-cG250-F(ab')$_2$ was administered intravenously into tumor bearing mice. The tumor xenografts were clearly visible in PET images acquired at 4 and 24 h p.i. Based on biodistribution studies, the tumor uptake of ^{89}Zr-cG250-F(ab')$_2$ was 3.71 $\pm$ 0.97%ID/g and 1.66 $\pm$ 0.48%ID/g at 4 h and 24 h p.i. The T:B and T:M ratios were 8.7 and 7.4 at 24 h p.i., respectively. The uptake in tumor correlated to pimonidazole staining ($r = 0.46$–0.68) and CA-IX expression ($r = 0.57$–0.74). Recently, Huizing et al. evaluated ^{111}In-DTPA-cG250-F(ab')$_2$ in two other head and neck squamous cell carcinoma models: SCCNij153 and SCCNij202 (Huizing et al. 2019). There was good concordance between SPECT image, autoradiography, and immunofluorescence. The uptake of ^{111}In-DTPA-cG250-F(ab')$_2$ in SCCNij153 tumors was 3.0 $\pm$ 1.5%ID/g and 3.0 $\pm$ 1.8%ID/g at 4 h and 24 h p.i., respectively. At 24 h p.i., T:B and T:M ratios were 19 $\pm$ 15 and 8.7 $\pm$ 1.9.

12.5.2 Radioimmunotherapy with G250/cG250

Divgi et al. conducted a phase I/II RIT dose escalation study with ^{131}I-mAbG250 (Divgi et al. 1998). Thirty-three patients with metastatic ccRCC were intravenously administered ^{131}I-mAbG250 (1110, 1665, 2220, 2775, or 3330 MBq/m^2; 10 mg) as a single dose. At doses above 1665 MBq/m^2, transient elevation of hepatic enzymes indicating impaired liver function was observed but not considered dose-limiting. The maximum tolerated dose (MTD) was determined to be 3330 MBq/m^2, based on hematological toxicity. Disease stabilization lasting more than 2 mo was observed

in 17 patients; patients were subsequently transferred to other therapies precluding follow-up. The development of human anti-mouse antibody (HAMA) response at 4 wk post-infusion in patients prevented retreatment.

G250 was chimerized to yield cG250, enabling a phase I study of ^{131}I-cG250 in patients with metastatic RCC (Steffens et al. 1999). Twelve patients were enrolled in the study, with each patient receiving a diagnostic dose (222 MBq; 0.5 mg). ^{131}I-cG250 showed similar biodistribution to ^{131}I-mAbG250, but less hepatic uptake was observed. Eight patients who had a positive scan received a therapeutic dose ranging from 1665 to 2775 MBq/m^2 (0.5 mg). The MTD was determined to be 2200 MBq/m^2, with dose-limiting hematological toxicity. One patient had stable disease for 3–6 mo, while another had partial response (50% reduction in lesion sizes) that lasted for at least 9 mo. The remaining 6 patients exhibited progressive disease. Of note, 1 patient who received two prior doses of 5 mg cG250 as part of an earlier clinical trial developed human anti-chimeric antibodies (HACA) in this study.

Divgi et al. explored the use of a dose fractionation approach for administration of ^{131}I-cG250 to prevent myeloablation and to improve response (Divgi et al. 2004). In this phase I trial, 15 metastatic RCC patients were enrolled and divided into groups of three. The first group was prescribed an average whole-body absorbed dose of 0.50 Gy, with succeeding groups receiving increased doses of 0.25 Gy increments. The first fraction of ^{131}I-cG250 was administered at 1110 MBq/5 mg, with subsequent fractions given at 2–3 d intervals. Imaging was used for dosimetry analysis. Patients who had no disease progression and demonstrated recovery from treatment toxicity were eligible for additional cycles; 5 patients qualified. Following treatment, 7 patients had stable disease, and 7 had disease progression. One patient developed sepsis during the study and was unable to continue treatment. HACA reactivity was observed in 2 patients. The fractionated approach did not significantly improve hematological toxicity or clinical outcomes.

Twenty-nine patients with metastatic RCC were recruited for a phase I study, in which participants received two sequential high doses of ^{131}I-cG250 (Brouwers et al. 2005). Baseline imaging identified 27 patients with adequate antibody accumulation in tumors for treatment. These patients were given a therapeutic dose of 2220 MBq/m^2, which was previously determined as the MTD. Patients were eligible for further treatment if they did not have grade 4 hematological toxicity or HACA response. Nineteen patients received another cycle of low dose diagnostic infusion and high dose therapeutic infusion of ^{131}I-cG250 (1110 MBq/m^2 to 1665 MBq/m^2). Fifteen patients completed treatments and were deemed assessable; 10 patients had progressive disease while 5 had stable disease ranging from 3–12 mo. Consistent with previous studies, the therapeutic efficacy of ^{131}I-cG250 was limited. The authors postulated that RIT with cG250 using metal radionuclides would improve tumor accumulation and retention.

Given the lack of clinical efficacy for ^{131}I-cG250, preclinical research on cG250 quickly shifted to other beta emitters ^{90}Y, ^{177}Lu, and ^{186}Re (Brouwers et al. 2004). ^{90}Y and ^{177}Lu are residualizing radionuclides and will remain inside the cell if internalized. Biodistribution and RIT studies were performed in mice bearing SK-RC-52 human ccRCC xenografts. ^{88}Y/^{125}I and ^{90}Y /^{131}I isotopes were used for

biodistribution and RIT studies, respectively. Depending on the chelator used, the cG250 conjugates radiolabeled with ^{88}Y and ^{177}Lu had approximately 8–10 times higher tumor accumulation than those labeled with ^{125}I or ^{186}Re. Tumor uptake for ^{177}Lu-SCN-Bz-DTPA-cG250, ^{177}Lu-DOTA-cG250, ^{88}Y-SCN-Bz-DTPA-cG250, ^{88}Y-DOTA-cG250, ^{125}I-cG250, and ^{186}Re-MAG$_3$-cG250 (MAG$_3$: mercaptoacetyl-triglycine) were 87.3 ± 14.0, 74.5 ± 10.5, 70.9 ± 8.4, 55.3 ± 10.7, 9.1 ± 2.0, and 7.9 ± 2.0%ID/g, respectively. At their respective MTDs, the calculated absorbed tumor dose for ^{177}Lu-SCN-Bz-DTPA-cG250 was 807 Gy, while other radioimmunoconjugates delivered between 76 and 104 Gy. ^{177}Lu-SCN-Bz-DTPA-cG250 delayed tumor growth by 186.4 ± 34.7 d compared to 26.6 ± 10.2 d for ^{131}I-cG250. The respective median survivals for the two groups were 294 d and 164 d, respectively.

^{177}Lu-DOTA-cG250 (^{177}Lu-cG250) was subsequently evaluated in a phase I trial by Stillebroer et al. (Fig. 12.3) (Stillebroer et al. 2013). DOTA was selected as it formed a more stable ^{177}Lu-chelator complex than DTPA according to the preclinical study. Twenty-three patients with progressive metastatic RCC were recruited for the study and divided into groups of three or more. The first dose level was 1110 MBq/m^2,

(a) Day 7 postinjection 185 MBq/10 mg ^{111}In-cG250   (b) Day 6 postinjection 1887 MBq/10 mg ^{177}Lu-cG250
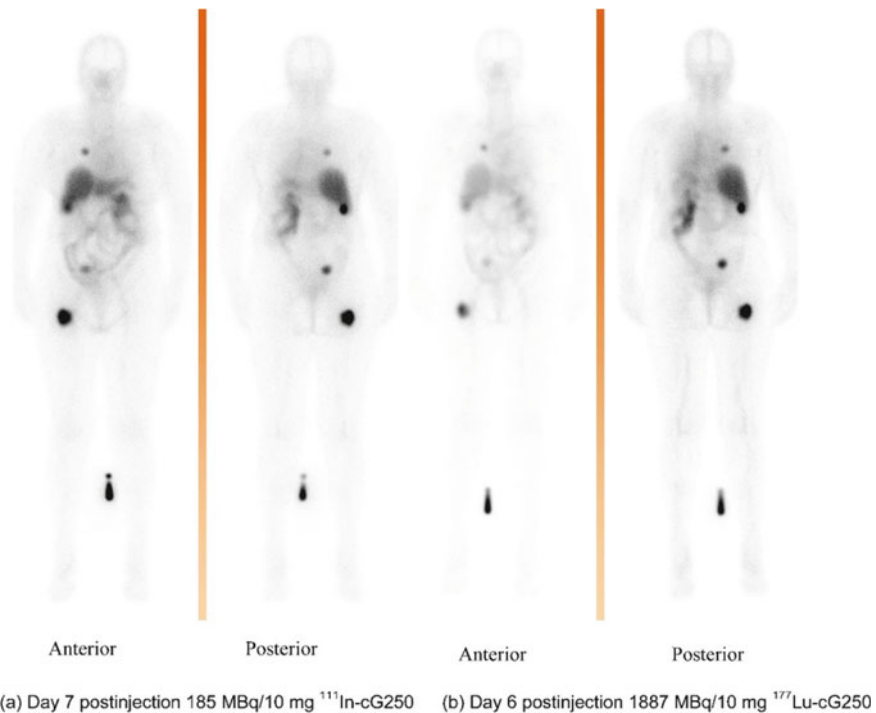
Fig. 12.3 Visualization of ccRCC metastases in lung, abdomen, and pelvis in a patient by immunoscintigraphy. **a** ^{111}In-DOTA-cG250 immunoscintigram of a patient with metastatic ccRCC acquired 7 d after injection of 185 MBq. **b** ^{177}Lu-cG250 immunoscintigram of the same patient acquired 6 d after injection of 1887 MBq. Figure adapted with permissions from Stillebroer et al. (2013)

and successive groups received increased dose increments of 370 MBq/m^2. MTD based on hematological toxicity was 2405 MBq/m^2. Similar to previous trials, patients were retreated if no disease progression was observed and recovery from hematological toxicity was demonstrated. Subsequent dose(s) was given at 75% of the previous dose level. Nine patients received 2 cycles and 4 patients received 3 cycles of ^{177}Lu-cG250. Three months after the first cycle, 17 patients had stable disease, but several patients progressed after receiving a second or third cycle. One patient showed partial response lasting 9 mo after two cycles of ^{177}Lu-cG250.

The latest evaluation of ^{177}Lu-cG250 was a phase II study by Muselaers et al. (2016). Fourteen patients received an infusion of 2405 MBq/m^2 ^{177}Lu-cG250. Similar to the phase I study, patients received additional cycles of RIT at 75% of the previous dose if they have no progressive disease and show recovery from toxicity. Only 6 patients received two cycles of RIT and none received a third cycle due to prolonged thrombocytopenia and/or neutropenia. After the first cycle, 8 patients had stable disease and 1 had partial response. Although ^{177}Lu-cG250 was able to stabilize disease progression, further reduction of treatment-associated toxicity is needed before it can be integrated into clinical practice.

12.5.3 Dual Modality Imaging with cG250

Muselaers et al. reported the synthesis and evaluation of ^{111}In-DTPA-cG250-IRDye800CW, a cG250 derivative that can be used for dual SPECT and near infrared fluorescence (NIRF) imaging (Muselaers et al. 2015). The radioactivity allows for preoperative localization of disease by SPECT imaging and for intraoperative detection of residual disease after resection by hand-held gamma probes. NIRF imaging helps surgeons to delineate surgical margins, supplementing the auditory cues from gamma detection. ^{111}In-DTPA-cG250-IRDye800CW was intravenously injected into nude mice bearing intraperitoneal SK-RC-52 ccRCC xenografts. Image acquisition was performed 48 h after tracer administration. Peak uptake in tumor, 58.5 ± 18.7%ID/g, was observed in those established 1 wk post-administration. The good concordance between SPECT and fluorescence images supports the utility of this dual-modality agent.

In a phase I study, Hekman et al. evaluated the safety and feasibility of ^{111}In-DOTA-G250-IRDye800CW for intraoperative dual-modality imaging (Fig. 12.4) (Hekman et al. 2018b). This cG250 derivative differs from the one studied by Muselaers et al. as it employs DOTA as the chelator instead of DTPA. Fifteen patients were included in this study, and different dose levels (5, 10, 30, or 50 mg, $n \geq 3$) of ^{111}In-DOTA-G250-IRDye800CW were administered intravenously. SPECT/CT imaging was performed 4 days p.i., and surgery was performed 6–7 d p.i. with the assistance of a gamma probe and a NIRF camera. No severe study-related adverse events were observed indicating safety of this agent. All cases of ccRCC were visible on SPECT/CT and localizable by gamma probe (T:K ratio of 2.5 ± 0.8). In contrast,
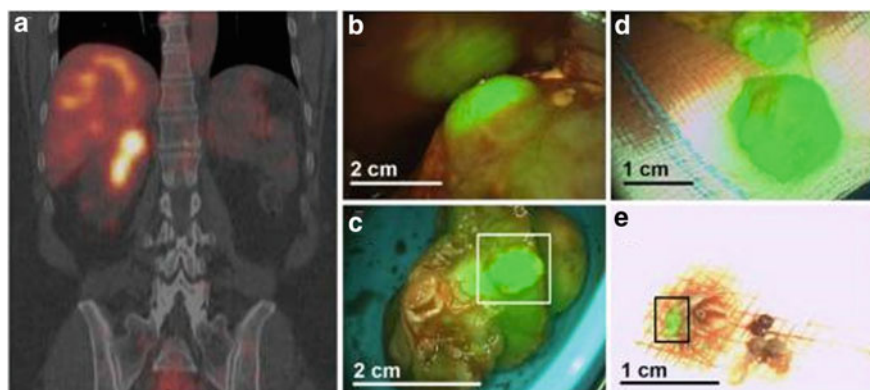
Fig. 12.4 Dual modality imaging after injection of ^{111}In-DOTA-cG250-IRDye800CW. **a** Preoperative SPECT/CT confirming presence of a CA-IX expressing ccRCC. **b** Intraoperative NIRF showed hyperfluorescence of tumor. **c** Assessment of the resected tumor specimen with NIRF suggested tumor within the surgical margin (square), which was subsequently confirmed by histopathology. **d** NIRF demonstrated that further resection contained vital tumor, again confirmed by histopathology. **e** NIRF was used to assess presence of tumor (square) in additional resected tissues. Histology confirmed that the fragment consisted mostly of fibrotic tissue, but also a 2 mm tumor. Scale bars are approximations. Figure adapted with permissions from Hekman et al. (2018b) in accordance with the Creative Commons Attribution (CC BY-NC 4.0) license

the T:K ratio for CA-IX non-expressing tumors was 1.0 ± 0.1. NIRF greatly aided in tumor delineation and assessing residual disease in surgical cavity.

12.6 Peptides and Affibodies

Peptides are commonly used in nuclear medicine as delivery vectors to target receptors overexpressed in various cancer subtypes (Fani and Maecke 2012). Peptides can bind rapidly to tumor and clear from non-target tissues. The pharmacokinetics, stability, and targeting of peptides can be optimized by using different combinations of radionuclides, linkers, amino acids, and structural configurations. Phage display peptide libraries were used to identify CA-IX binders. Askoxylakis et al. identified a dodecapeptide, YNTNHVPLSPKY (CaIX-P1), that binds to the extracellular domain of CA-IX (Askoxylakis et al. 2010). The *N*-terminal tyrosine was used for ^{125}I/^{131}I radiolabeling. ^{131}I-CaIX-P1 was evaluated in ccRCC SK-RC-52 xenograft mice. From biodistribution study, tumor uptake at 1 h p.i. was ~2.5%ID/g and decreasing thereafter. The highest contrast for ^{131}I-CaIX-P1 was at 1 h p.i., when T:B and T:M ratios were 0.65 ± 0.24 and 4.11 ± 2.44, respectively. The peptide was unstable in plasma, and had a half-life of 25 min.

To optimize stability and targeting properties of CaIX-P1, Rana et al. performed alanine panning and peptide truncation studies (Rana et al. 2012). They identified

NHVPLSPy (CaIX-P1-4-10) as the minimal sequence necessary for CA-IX binding. A D-tyrosine residue was added at the *C*-terminus for radiolabeling purposes. In vitro, CaIX-P1-4-10 showed serum stability of 90 min, and 5.8 times higher uptake in cells compared to CaIX-P1. However, this peptide was unable to delineate SK-RC-52 xenografts from background tissues despite showing good uptake (~2.5%ID/g at 1 h p.i.). The IC_{50} value for CaIX-P1-4-10 against CA-IX was later determined to be in the micromolar range. Recently, Jia et al. synthesized an ^{18}F-fluorine derivative of CaIX-P1 and evaluated its uptake properties in the hypoxia HT-29 tumor model (Jia et al. 2019). An ^{18}F-labeled azide prosthetic group was used for click chemistry with the terminal alkyne group for radiolabeling (^{18}F-CA-IX-P1-4-10). PET imaging studies were conducted, but minimal uptake was observed in tumor.

The Heidelberg group which isolated CaIX-P1 performed a secondary phage display to isolate another dodecapeptide NMPKDVTTRMSS (PGLR-P1) (Rana et al. 2013). To improve isoform selectivity, the PG-like domain of CA-IX was used as the bait in this set up. Once again, a D-tyrosine residue was added to the *C*-terminus for radiolabeling with ^{125}I/^{131}I. In vitro studies indicated that binding affinity for CA-IX was in the micromolar range. SK-RC-52 tumor xenografts showed low uptake (0.48 ± 0.20%ID/g at 1 h p.i.), and no contrast was observed. While these short peptides have limited application for CA-IX targeting, another class of peptide-based probes (affibodies) have been far more successful.

Affibodies are protein scaffolds developed from the immunoglobulin G binding domain of staphylococcal protein A (Feldwisch and Tolmachev 2012). An affibody molecule is ~ 6–7 kDa in molecular weight depending on the composition. Each affibody contains 58 amino acids, of which 13 are responsible for mediating nano or picomolar binding to a target of interest. Affibodies are less sensitive to temperature and pH and have faster pharmacokinetics than mAbs. Honarvar et al. used an affibody library to identify a CA-IX targeting affibody (ZCAIX:1) for imaging ccRCC (Honarvar et al. 2015). ZCAIX:1 was radiolabeled with ^{99m}Tc and ^{125}I for comparison. SPECT imaging and biodistribution studies were performed in mice bearing SK-RC-52 xenografts. The binding affinity of ^{99m}Tc-(HE)$_3$-ZCAIX:1 for SK-RC-52 cells was determined to be 1.3 nM. Following intravenous injection, ^{99m}Tc-(HE)$_3$-ZCAIX:1 showed high and rapid uptake in tumor (22.3 ± 3.2%ID/g at 1 h p.i.). The uptake in tumor dropped to 9.7 ± 0.7%ID/g and 7.3 ± 3.0%ID/g at 4 h and 8 h p.i., respectively. The highest T:B and T:M ratios were 53 ± 10 and 104 ± 52 observed at 4 h p.i. Kidney uptake was >100% ID/g at all timepoints. With a non-residualizing radionuclide, renal uptake of ^{125}I-(HE)$_3$-ZCAIX:1 was significantly lower (2.7 ± 1.4%ID/g at 6 h p.i.); however, this was accompanied by a decrease in tumor uptake (2.2 ± 1.4%ID/g at 6 h p.i.). The data suggests that ^{99m}Tc-(HE)$_3$-ZCAIX:1 has the potential for imaging extrarenal lesions that express CA-IX.

Garousi et al. performed a comparison study with ZCAIX:1 and three novel affibody variants (ZCAIX:2, ZCAIX:3, and ZCAIX:4) for CA-IX imaging (Fig. 12.5) (Garousi et al. 2016). The new variants showed nanomolar binding affinity (K_D: 1.2–7.3 nM) for SK-RC-52 cells. The affibodies were radiolabeled with ^{99m}Tc and ^{125}I. The uptake in SK-RC-52 tumors ranged from 4.3 ± 0.7%ID/g to 16.3 ± 0.9%ID/g at 4 h p.i. for the ^{99m}Tc-labeled derivatives. At this time point, ^{99m}Tc-(HE)$_3$-ZCAIX:2

Fig. 12.5 Maximum
intensity projections of
microSPECT/CT using
CA-IX targeting affibodies at
4 h p.i. **a** Imaging using
^{99m}Tc-(HE)$_3$-ZCAIX:2. The
linear color scale was
adjusted to provide clear
visualization of a tumor. **b**
Imaging using
^{125}I-(HE)$_3$-ZCAIX:4. Full
linear color scale was
applied. Figure adapted with
permission from Garousi
et al. (2016). Copyright 2016
American Chemistry Society
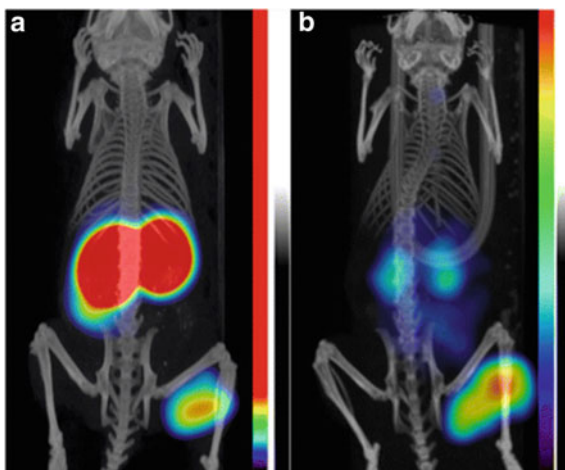
showed the highest contrast ratios (T:B of 44 ± 7 and T:M of 109 ± 11). Consistent
with previous study, high renal retention (>100%ID/g) was observed for all time
points. On the other hand, the ^{125}I-labeled derivates showed 5–50 times less uptake
(4–22%ID/g at 4 h p.i.) in kidneys. ^{125}I-ZCAIX:2 had the highest tumor uptake (19
$\pm$ 2%ID/g) at 4 h p.i., which corresponded to T:B and T:M ratios of 21 ± 5 and
129 ± 42, respectively. The authors concluded that the pairing of a non-residualizing
radionuclide with an affibody may be useful for imaging primary ccRCC.

12.7 Small Molecule Inhibitors

Small molecule inhibitors are the most diverse group of antigen recognition
molecules for CA-IX targeting. Most small molecule inhibitors that have been
explored for imaging/therapy are sulfonamide derivatives. Sulfonamides inhibit CA-
IX by forming coordination with the zinc ion and displacing water in the catalytic
domain (Supuran et al. 2001). The major challenge for developing small molecule-
based theranostic agents for CA-IX is selectivity since the catalytic domain is rela-
tively conserved between isoforms (Alterio et al. 2012). There are three extracel-
lular CA isoenzymes: CA-IX, CA-XII, and CA-XIV. To confer CA-IX selectivity,
successful radiopharmaceuticals generally have features that render them cell imper-
meable (Alterio et al. 2012). Even when selectivity is achieved, some tracers have
been hampered by low uptake or instability (Lau et al. 2014).

12.7.1 Net Charge

^{18}F-VM4-037 is an ethoxzolamide derivative developed for CA-IX PET imaging and remains the only small molecule inhibitor to advance to clinical studies (Doss et al. 2014). ^{18}F-VM4-037 has a free carboxylate group that is deprotonated at physiological pH. When this occurs, the negative charge restricts entry of the molecule into the cell conferring selectivity for CA-IX. Doss et al. reported the biodistribution and dosimetry of ^{18}F-VM4-037 in healthy volunteers in a phase I study (Doss et al. 2014). From PET images, ^{18}F-VM4-037 was immediately taken up by the liver and kidneys with minimal clearance (4% through kidneys) during the 133 min study period. Almost 50% of the dose were sequestered by these two organs. Based on a 370 MBq dose, the predicted effective dose for a patient was 10 ± 0.5 mSv. The kidneys would receive 101 ± 11 mGy, while the liver would receive 89 ± 25 mGy.

Turkbey et al. evaluated ^{18}F-VM4-037 in a phase II study with 11 RCC patients (Turkbey et al. 2016). Ten patients had histology-confirmed ccRCC, and 2 patients had metastatic lesions. Primary lesion detection of ^{18}F-VM4-037 (tumor SUV_{mean}: 3.04) was obscured by high uptake in normal renal parenchyma (kidney SUV_{mean}: 35.4). While primary lesions were difficult to ascertain without CT, extrarenal lesions in patients with metastasis were readily identified (SUV_{max}: 5.92). Since preclinical data for ^{18}F-VM4-037 was previously unpublished, Peeters et al. synthesized ^{18}F-VM4-037 and evaluated its ability to image CA-IX expression in the U373 human glioma and HT-29 human colorectal xenograft models (Peeters et al. 2015). Consistent with the clinical studies, ^{18}F-VM4-037 showed high accumulation in the liver and kidneys. However, no uptake was observed in either tumor model raising questions about the sensitivity of ^{18}F-VM4-037 for targeting CA-IX in vivo. In this study, the K_i of ^{18}F-VM4-037 for CA-IX was found to be 0.12 µM.

Our research group reported the synthesis and evaluation of an ^{18}F-labeled cationic sulfonamide derivative (Zhang et al. 2017). The cationic quaternary ammonium group maintains a net positive charge, conferring selectivity for CA-IX. Biodistribution and PET imaging studies were performed in HT-29 tumor xenograft mice. Tumor uptake was 0.41 ± 0.06%ID/g at 1 h p.i., and corresponded to T:B and T:M ratios of <2. HT-29 tumors were visible in PET images despite the low absolute uptake. Although contrast was less than that of the other sulfonamides, results were encouraging considering the modest affinity for CA-IX. The compound had a K_i value of 0.22 µM for CA-IX.

12.7.2 Multivalence and Size

In addition to incorporating net charge, our group successfully leveraged a multivalent approach to confer in vivo selectivity for CA-IX (Lau et al. 2015). We hypothesized that a trimeric sulfonamide inhibitor would have sufficient bulk (>1 kDa)

to restrict intracellular entry. To achieve this, we first prepared azide derivatives of two CA inhibitors, 4-(2-aminoethyl)benzenesulfonamide (AEBS) and 4-aminobenzensulfonamide (ABS). These inhibitors were subsequently conjugated to a radio-prosthetic group containing three alkyne groups and an ammoniomethyltrifluoroborate (AmBF$_3$) moiety to form ^{18}F-AmBF$_3$-(AEBS)$_3$ and ^{18}F-AmBF$_3$-(ABS)$_3$. Biodistribution and PET imaging studies were performed in HT-29 tumor-bearing mice. For the two compounds, tumor uptake was 0.30–0.33%ID/g at 1 h p.i., which was 5 times higher than the activity in blood (0.07–0.09%ID/g). CA-I and CA-II are off-target isoenzymes that are expressed in the cytosol of red blood cells. Tumors were clearly visible in PET images, and the T:B (3.93 $\pm$ 1.26) and T:M (9.55 $\pm$ 2.96) ratios were the highest reported small molecule-based imaging of CA-IX at the time of publication. ^{18}F-AmBF$_3$-(AEBS)$_3$ and ^{18}F-AmBF$_3$-(ABS)$_3$ had K$_i$ values of 35.7 nM and 8.5 nM, respectively.

12.7.3 Radiometal Chelator Complex

Rami et al. demonstrated that sulfonamides conjugated to polyaminocarboxylate chelators (e.g., DTPA and DOTA) are unable to penetrate red blood cells (Rami et al. 2008). This observation spurred our group to synthesize three ^{68}Ga-labeled sulfonamide derivatives with different chelators (Fig. 12.6) (Lau et al. 2016). Monomeric (Ga-DOTA-AEBSA), dimeric (Ga-DOTA-(AEBSA)$_2$), and trimeric (Ga-NOTGA-(AEBSA)$_3$; NOTGA: 1,4,7-triazacyclononane-1,4,7-tris-(glutaric acid)) derivatives were prepared. Biodistribution and PET imaging studies were performed in HT-29 tumor xenograft mice. Tumor uptake ranged from 0.81 to 2.30%ID/g at 1 h p.i. and positively correlated to the number of targeting moieties and molecular weight. The monomer cleared predominantly through the kidneys, while the dimer and trimer were cleared by the renal and hepatobiliary pathways. ^{68}Ga-DOTA-AEBSA exhibited the lowest tumor uptake but had the highest contrast (T:M ratio: 5.02 $\pm$ 0.22) due its favorable pharmacokinetics. Good-contrast PET images were generated by all three derivatives. ^{68}Ga-DOTA-AEBSA showed heterogeneous distribution in tumors and areas of focal uptake. The K$_i$ values of the three compounds ranged from 7.7 nM to 25.4 nM.

Following a similar strategy, Sneddon et al. synthesized a monomeric ^{68}Ga-DOTA-sulfonamide derivative (Sneddon et al. 2016). Instead of directly conjugating the sulfonamide group to one of the carboxylic groups in DOTA, the authors inserted a polyethylene glycol linker as a pharmacokinetic modifier. In vivo evaluations were conducted in mice bearing HCT116 human colorectal cancer xenografts. Tumors were visible in PET images at 1 h p.i.; however, the uptake was not retained and there was washout of signal by 2 h p.i. Absolute uptake values were not reported, but the T:B ratio was reportedly 2.36 $\pm$ 0.42 at 1 h p.i. Compared to ^{68}Ga-DOTA-AEBSA, the K$_i$ value of this monomeric compound was higher at 63.1 nM.

Krall et al. reported the synthesis and evaluation of a ^{99m}Tc-labeled acetazolamide derivative (Krall et al. 2016). The tracer contained an acetazolamide derivative, a
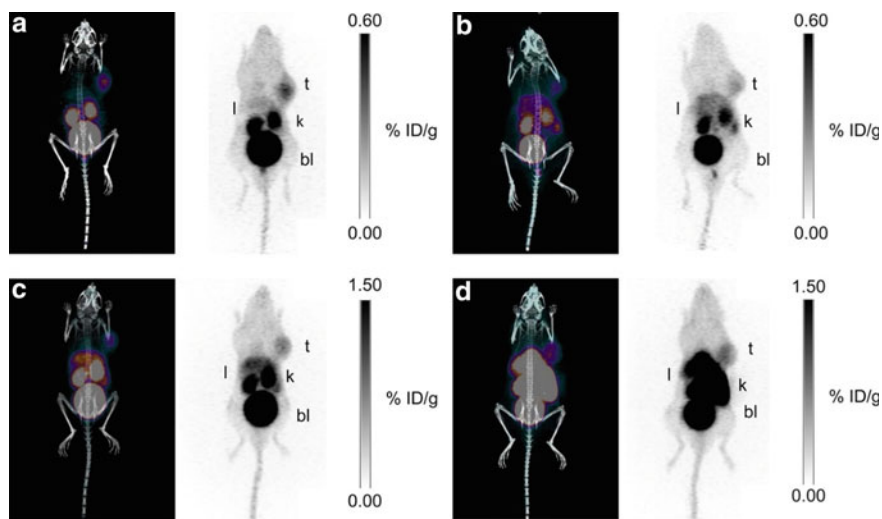
Fig. 12.6 Maximal intensity projection images of PET/CT and PET with ^{68}Ga tracers at 1 h p.i. **a** ^{68}Ga-DOTA-AEBSA; **b** ^{68}Ga-DOTA-AEBSA preblocked with 10 mg/kg of acetazolamide; **c** ^{68}Ga-DOTA-(AEBSA)$_2$; **d** ^{68}Ga-NOTGA-(AEBSA)$_3$. Tumor uptake was observed for all three compounds with ^{68}Ga-DOTA-AEBSA displaying highest contrast. t = tumor; l = liver; k = kidney; bl = bladder. Figure adapted with permissions from Lau et al. (2016). Copyright 2016 American Chemistry Society

triazine-based linker, and a Lys-Asp-Cys motif for ^{99m}Tc-labeling. In vivo evaluations were performed in the SK-RC-52 ccRCC model that overexpresses CA-IX. Based on biodistribution studies, tumor uptake peaked at 3 h p.i. at 22.1 ± 0.16%ID/g with a T:B ratio of 69.9 ± 0.21. Unlike other small molecules that washout from tumor, uptake was well retained by 6 h p.i. (19.8 ± 0.13%ID/; T:B ratio of 100 ± 0.94). SPECT images showed clear delineation of tumors from background tissues. While not directly measured, it was assumed that the compound had nanomolar binding affinity to CA-IX since acetazolamide was used as the targeting pharmacophore.

Wichert et al. identified a novel dual motif CA-IX inhibitor from a DNA encoded chemical library (Wichert et al. 2015). This inhibitor consists of an acetazolamide and a 4,4-bis(4-hydroxyphenyl)valeric acid; the binding site of the latter remains unknown. The Pomper group radiolabeled this inhibitor by adding either an ^{111}In-DOTA or ^{64}Cu-NOTA (NOTA:1,4,7-triazacyclononane-1,4,7-triacetic acid) complex for ccRCC imaging (Yang et al. 2015; Minn et al. 2016). Biodistribution and imaging studies were performed in mice bearing SK-RC-52 xenografts. For ^{111}In-XYIMSR-01, maximal tumor uptake was observed at 8 h p.i. (34.0 ± 15.2%ID/g) with corresponding T:B and T:M ratios of 77.0 ± 32.5 and 34.2 ± 16.0. Tumor uptake of ^{111}In-XYIMSR-01 decreased slightly to 25.6 ± 17.7%ID/g at 24 p.i., while T:B and T:M ratios improved to 178.1 ± 145.4 and 68.4 ± 29.0. For ^{64}Cu-XYIMSR-06, maximal tumor uptake was observed at 4 h p.i. (19.3 ± 4.51%ID/g) with corresponding T:B and T:M ratios of 57.7 ± 9.3, and 29.4 ± 9.9. Similarly, tumor uptake

decreased to 6.23 $\pm$ 1.41%ID/g by 24 h p.i., but T:B and T:M ratios improved to 142.6 $\pm$ 115.8 and 261.3 $\pm$ 47.3. Based on imaging modality and faster pharmacokinetics, ^{64}Cu-XYIMSR-06 is likely more favorable for translation despite the lower absolute tumor uptake.

More recently, Yang et al. synthesized ^{64}Cu-XYIMSR-06 and evaluated its ability to image the orthotopic U87 MG glioblastoma model (Fig. 12.7) (Yang et al. 2019). Due to lower expression of CA-IX in this hypoxia model, maximal tumor uptake was 3.13 $\pm$ 0.26%ID/g with T:B and T:M ratios of 7.67 $\pm$ 1.08 and 3.01 $\pm$ 0.68. The tumor-to-brain ratio was 4.46 $\pm$ 0.86. From PET images, orthotopic xenografts were readily visualized at 2 h and 8 h p.i. While initial results look promising, the ability of ^{64}Cu-XYIMSR-06 to effectively cross the blood–brain-barrier (BBB) needs to be further assessed. The BBB is generally disrupted during the establishment of glioma models. The binding affinity of ^{64}Cu-XYIMSR-06 for the U87 MG cell line was determined to be 4.22 nM.

Iikuni et al. developed three ureidosulfonamide-based inhibitors for SPECT imaging and radioligand therapy (Iikuni et al. 2018). Ureidosulfonamides have better binding affinity for CAs compared to unsubstituted sulfonamides. The authors synthesized a monovalent inhibitor conjugated to a DOTA chelator for ^{111}In-labeling (^{111}In-US1), and a bivalent inhibitor conjugated to DOTA for ^{111}In/^{90}Y-labeling (^{111}In/^{90}Y-US2). Biodistribution studies were performed in mice bearing both HT-29 colorectal cancer (high CA-IX expression) and MDA-MB-231 (low CA-IX expression) breast cancer xenografts. ^{111}In-US2 showed higher uptake in both models compared to ^{111}In-US1. HT-29 tumor uptake of ^{111}In-US2 peaked at 1 h p.i. at 4.57 $\pm$ 0.21%ID/g (T:B and T:M ratios of 1.11 $\pm$ 0.16 and 2.86 $\pm$ 0.43) and decreased gradually over the course of the study. The uptake in MDA-MB-231 tumor was lower than HT-29 tumor at all time points. Radioligand therapy with ^{90}Y-US2 (1.85, 3.7 and 7.4 MBq) was performed in mice bearing only HT-29 tumors. The administration of ^{90}Y-US2 led to inhibition of HT-29 tumor growth, in a dose-dependent manner. This is one of the first endoradiotherapy studies targeting CA-IX using a small molecule inhibitor.

12.8   Perspectives and Conclusion

CA-IX represents as a theranostic target for all solid tumors, especially for ccRCCs where CA-IX expression is mainly driven by genetic aberrations in lieu of oxygen availability. According to the 2018 GLOBOCAN report, there were over 400,000 new incidences of ccRCC worldwide with over 175,000 associated mortalities (Bray et al. 2018). cG250 and its derivatives are promising for targeting ccRCCs because they clear through the hepatobiliary system. This reduces background when attempting to image primary or recurrent lesions. A multi-center phase III study to investigate the sensitivity and specificity of [89]Zr-cG250 for ccRCC has begun recruitment (ClinicalTrials.gov Identifier: NCT03849118). It is anticipated that this compound will displace [124]I-cG250 as the imaging agent of choice. In terms of RIT with cG250,
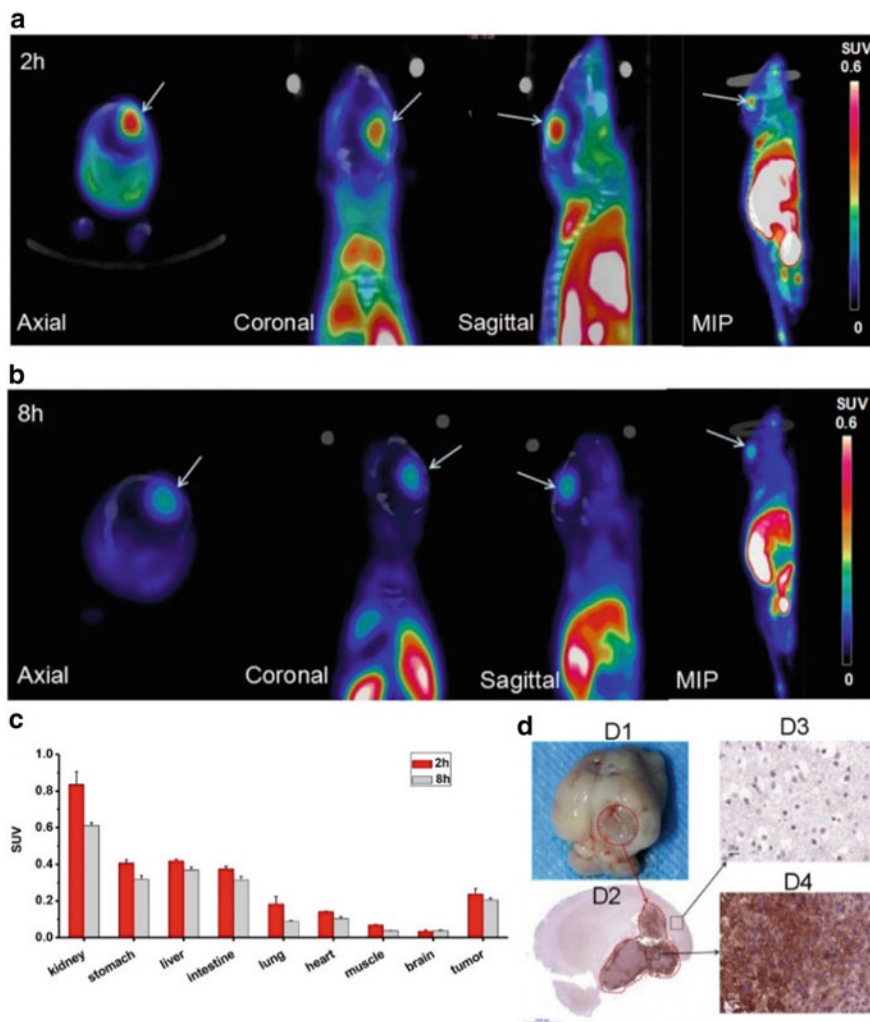
Fig. 12.7 PET images of orthotopic U87 MG xenografts after injection of ^{64}Cu-XYIMSR-06. **a, b** Detection of the intracranial tumor at 2 and 8 h after injection. Arrows indicate the tumor. **c** SUV values for selected organs based on drawn ROIs. **d** Orthotopic glioma and immunohistochemistry. (**D1**) Tumor in the right cerebral hemisphere in red circle. (**D2**) CA-IX immunohistochemical staining. (**D3**) CA-IX expression is absent in normal brain tissue. (**D4**) CA-IX expression tumor tissue (40 × magnification of original micrographs). Figure adapted with permissions from Yang et al. (2019). Copyright 2016 American Chemistry Society

myelotoxicity must be safely mitigated or controlled. Since ^{177}Lu has imageable photons, personalized dosing based on imaging dosimetric analyses is one way to reduce toxicity. Merkx et al. recently disclosed the development of [225]Ac-cG250 at a conference proceeding (Merkx et al. 2019). [225]Ac is an alpha particle emitter and is able to induce more dsDNA breakages in cancer cells than ^{177}Lu, which is a beta particle emitter (Kozempel et al. 2018). At the same time, the particle range of [225]Ac is limited which helps to reduce off-target toxicity.

While the other classes of CA-IX radiopharmaceuticals can also be used for ccRCC, they are more ideal for targeting hypoxic niches. The barriers for small molecule inhibitors have been low uptake and subsequent retention in tumors. However, recent work by Krall et al. and Yang et al. demonstrate that these challenges can be met by structure–activity relationship optimization. As more potent and selective inhibitors are discovered (Dudutiene et al. 2014), we anticipate that there will be continued interest in advancing small molecule-based agents for CA-IX. Hypoxic tumors are difficult to treat with monotherapy; therefore, combinatorial treatments are necessary especially for disseminated disease. Small molecule inhibitors can be used to target CA-IX in combination with other agents like tyrosine kinase inhibitors (Oosterwijk-Wakka et al. 2011) or immune checkpoint inhibitors (Chafe et al. 2019). Radiotherapeutic agents derived from small molecules are likely to be less toxic because they have faster clearance and are non-immunogenic, compared to RIT. In summary, given the multifaceted role CA-IX has in cancer biology, CA-IX theranostic agents have the potential to ameliorate cancer management and patient outcomes.

References

Ahlskog JKJ, Schliemann C, Mårlind J, Qureshi U, Ammar A, Pedley RB, Neri D (2009) Human monoclonal antibodies targeting carbonic anhydrase IX for the molecular imaging of hypoxic regions in solid tumours. Br J Cancer 101:645–657

Alterio V, Di Fiore A, D'Ambrosio K, Supuran CT, De Simone G (2012) Multiple binding modes of inhibitors to carbonic anhydrases: how to design specific drugs targeting 15 different isoforms? Chem Rev 112:4421–4468

Askoxylakis V, Garcia-Boy R, Rana S, Krämer S, Hebling U, Mier W, Altmann A, Markert A, Debus J, Haberkorn U (2010) A new peptide ligand for targeting human carbonic anhydrase IX, identified through the phage display technology. PLoS One 5:e15962

Bennewith KL, Dedhar S (2011) Targeting hypoxic tumour cells to overcome metastasis. BMC Cancer 11:504

Bray F, Ferlay J, Soerjomataram I, Siegel RL, Torre LA, Jemal A (2018) Global cancer statistics 2018: GLOBOCAN estimates of incidence and mortality worldwide for 36 cancers in 185 countries. CA Cancer J Clin 68:394–424

Brouwers AH, Buijs WCAM, Oosterwijk E, Boerman OC, Mala C, De Mulder PHM, Corstens FHM, Mulders PFA, Oyen WJG (2003) Targeting of metastatic renal cell carcinoma with the chimeric monoclonal antibody G250 labeled with 131I or 111In: an intrapatient comparison. Clin Cancer Res 9:3953S-S3960

Brouwers AH, van Eerd JEM, Frielink C, Oosterwijk E, Oyen WJG, Corstens FHM, Boerman OC (2004) Optimization of radioimmunotherapy of renal cell carcinoma: labeling of monoclonal antibody cG250 with 131I, 90Y, 177Lu, or 186Re. J Nucl Med 45:327–337

Brouwers AH, Mulders PFA, De Mulder PHM, Van Den Broek WJM, Buijs WCAM, Mala C, Joosten FBM, Oosterwijk E, Boerman OC, Corstens FHM, Oyen WJG (2005) Lack of efficacy of two consecutive treatments of radioimmunotherapy with 131I-cG250 in patients with metastasized clear cell renal cell carcinoma. J Clin Oncol 23:6540–6548

Carlin S, Khan N, Ku T, Longo VA, Larson SM, Smith-Jones PM (2010) Molecular targeting of carbonic anhydrase ix in mice with hypoxic HT29 colorectal tumor xenografts. PLoS One 5:e10857

Čepa A, Ráliš J, Král V, Paurová M, Kučka J, Humajová J, Lázníček M, Lebeda O (2018) In vitro evaluation of the monoclonal antibody 64Cu-IgG M75 against human carbonic anhydrase IX and its in vivo imaging. Appl Radiat Isot 133:9–13

Chafe SC, McDonald PC, Saberi S, Nemirovsky O, Venkateswaran G, Burugu S, Gao D, Delaidelli A, Kyle AH, Baker JHE, Gillespie JA, Bashashati A, Minchinton AI, Zhou Y, Shah SP, Dedhar S (2019) Targeting hypoxia-induced carbonic anhydrase IX enhances immune checkpoint blockade locally and systemically. Cancer Immunol Res canimm.0657.2018

Chamie K, Donin NM, Klöpfer P, Bevan P, Fall B, Wilhelm O, Störkel S, Said J, Gambla M, Hawkins RE, Jankilevich G, Kapoor A, Kopyltsov E, Staehler M, Taari K, Wainstein AJA, Pantuck AJ, Belldegrun AS (2017) Adjuvant weekly girentuximab following nephrectomy for high-risk renal cell carcinoma: the ARISER randomized clinical trial. JAMA Oncol 3:913–920

Chiavenna SM, Jaworski JP, Vendrell A (2017) State of the art in anti-cancer mAbs. J Biomed Sci 24:15

Chrastina A, Závada J, Parkkila S, Kaluz Š, Kaluzová M, Rajčáni J, Pastorek J, Pastoreková S (2003) Biodistribution and pharmacokinetics of 125I-labeled monoclonal antibody M75 specific for carbonic anhydrase IX, an intrinsic marker of hypoxia, in nude mice xenografted with human colorectal carcinoma. Int J Cancer 105:873–881

Clark PE (2009) The role of VHL in clear-cell renal cell carcinoma and its relation to targeted therapy. Kidney Int 76:939–945

Divgi CR, Bander NH, Scott AM, O'Donoghue JA, Sgouros G, Welt S, Finn RD, Morrissey F, Capitelli P, Williams JM, Deland D, Nakhre A, Oosterwijk E, Gulec S, Graham MC, Larson SM, Old LJ (1998) Phase I/II radioimmunotherapy trial with iodine-131-labeled monoclonal antibody G250 in metastatic renal cell carcinoma. Clin Cancer Res 4:2729–2739

Divgi CR, O'Donoghue JA, Welt S, O'Neel J, Finn R, Motzer RJ, Jungbluth A, Hoffman E, Ritter G, Larson SM, Old LJ (2004) Phase I clinical trial with fractionated radioimmunotherapy using 131I-labeled chimeric G250 in metastatic renal cancer. J Nucl Med 45:1412–1421

Divgi CR, Pandit-Taskar N, Jungbluth AA, Reuter VE, Gönen M, Ruan S, Pierre C, Nagel A, Pryma DA, Humm J, Larson SM, Old LJ, Russo P (2007) Preoperative characterisation of clear-cell renal carcinoma using iodine-124-labelled antibody chimeric G250 (124I-cG250) and PET in patients with renal masses: a phase I trial. Lancet Oncol 8:304–310

Divgi CR, Uzzo RG, Gatsonis C, Bartz R, Treutner S, Yu JQ, Chen D, Carrasquillo JA, Larson S, Bevan P, Russo P (2013) Positron emission tomography/computed tomography identification of clear cell renal cell carcinoma: results from the REDECT trial. J Clin Oncol 31:187–194

Doss M, Kolb HC, Walsh JC, Mocharla VP, Zhu Z, Haka M, Alpaugh RK, Chen DYT, Yu JQ (2014) Biodistribution and radiation dosimetry of the carbonic anhydrase IX imaging agent [18F]VM4-037 determined from PET/CT scans in healthy volunteers. Mol Imaging Biol 16:739–746

Dudutiene V, Matuliene J, Smirnov A, Timm DD, Zubriene A, Baranauskiene L, Morkunaite V, Smirnoviene J, Michailoviene V, Juozapaitiene V, Mickeviciute A, Kazokaite J, Bakšyte S, Kasiliauskaite A, Jachno J, Revuckiene J, Kišonaite M, Pilipuityte V, Ivanauskaite E, Milinaviciute G, Smirnovas V, Petrikaite V, Kairys V, Petrauskas V, Norvaišas P, Linge D, Gibieža P, Čapkauskaite E, Zakšauskas A, Kazlauskas E, Manakova E, Gražulis S, Ladbury JE, Matulis D (2014) Discovery and characterization of novel selective inhibitors of carbonic anhydrase IX. J Med Chem 57:9435–9446

Escudier B, Porta C, Schmidinger M, Rioux-Leclercq N, Bex A, Khoo V, Gruenvald V, Horwich A (2016) Renal cell carcinoma: ESMO clinical practice guidelines for diagnosis, treatment and follow-up†. Ann Oncol 27:v58–v68

Fani M, Maecke HR (2012) Radiopharmaceutical development of radiolabelled peptides. Eur J Nucl Med Mol Imaging 39:11–30

Feldwisch J, Tolmachev V (2012) Engineering of affibody molecules for therapy and diagnostics. Methods Mol Biol 899:103–126

Fleming IN, Manavaki R, Blower PJ, West C, Williams KJ, Harris AL, Domarkas J, Lord S, Baldry C, Gilbert FJ (2015) Imaging tumour hypoxia with positron emission tomography. Br J Cancer 112:238–250

Freise AC, Wu AM (2015) In vivo imaging with antibodies and engineered fragments. Mol Immunol 67:142–152

Garousi J, Honarvar H, Andersson KG, Mitran B, Orlova A, Buijs J, Löfblom J, Frejd FY, Tolmachev V (2016) Comparative evaluation of affibody molecules for radionuclide imaging of in vivo expression of carbonic anhydrase IX. Mol Pharm 13:3676–3687

Gorin MA, Rowe SP, Allaf ME (2015) Nuclear imaging of renal tumours: a step towards improved risk stratification. Nat Rev Urol 12:445–450

Harris AL (2002) Hypoxia—a key regulatory factor in tumour growth. Nat Rev Cancer 2:38–47

Hekman MCH, Rijpkema M, Aarntzen EH, Mulder SF, Langenhuijsen JF, Oosterwijk E, Boerman OC, Oyen WJG, Mulders PFA (2018a) Positron emission tomography/computed tomography with 89zr-girentuximab can aid in diagnostic dilemmas of clear cell renal cell carcinoma suspicion. Eur Urol 74:257–260

Hekman MC, Rijpkema M, Muselaers CH, Oosterwijk E, Hulsbergen-Van de Kaa CA, Boerman OC, Oyen WJ, Langenhuijsen JF, Mulders PF (2018b) Tumor-targeted dual-modality imaging to improve intraoperative visualization of clear cell renal cell carcinoma: a first in man study. Theranostics 8:2161–2170. https://doi.org/10.7150/thno.23335

Hilvo M, Baranauskiene L, Salzano AM, Scaloni A, Matulis D, Innocenti A, Scozzafava A, Monti SM, Di Fiore A, De Simone G, Lindfors M, Jänis J, Valjakka J, Pastoreková S, Pastorek J, Kulomaa MS, Nordlund HR, Supuran CT, Parkkila S (2008) Biochemical characterization of CA IX, one of the most active carbonic anhydrase isozymes. J Biol Chem 283:27799–27809

Hoeben BAW, Kaanders JHAM, Franssen GM, Troost EGC, Rijken PFJW, Oosterwijk E, Dongen GAMS, Oyen WJG, Boerman OC, Bussink J (2010) PET of hypoxia with 89Zr-labeled cG250-F(ab')2 in head and neck tumors. J Nucl Med 51:1076–1083

Holmquist-Mengelbier L, Fredlund E, Löfstedt T, Noguera R, Navarro S, Nilsson H, Pietras A, Vallon-Christersson J, Borg Å, Gradin K, Poellinger L, Påhlman S (2006) Recruitment of HIF-1α and HIF-2α to common target genes is differentially regulated in neuroblastoma: HIF-2α promotes an aggressive phenotype. Cancer Cell 10:413–423

Honarvar H, Garousi J, Gunneriusson E, Höidén-Guthenberg I, Altai M, Widström C, Tolmachev V, Frejd FY (2015) Imaging of CAIX-expressing xenografts in vivo using 99mTc-HEHEHE-ZCAIX:1 Affibody molecule. Int J Oncol 46:513–520

Hsieh JJ, Purdue MP, Signoretti S, Swanton C, Albiges L, Schmidinger M, Heng DY, Larkin J, Ficarra V (2017) Renal cell carcinoma. Nat Rev Dis Prim 3:17009

Huizing FJ, Hoeben BAW, Franssen GM, Boerman OC, Heskamp S, Bussink J (2019) Quantitative imaging of the hypoxia-related marker CAIX in head and neck squamous cell carcinoma xenograft models. Mol Pharm 16:701–708

Iikuni S, Ono M, Watanabe H, Shimizu Y, Sano K, Saji H (2018) Cancer radiotheranostics targeting carbonic anhydrase-IX with 111In- and 90Y-labeled ureidosulfonamide scaffold for SPECT imaging and radionuclide-based therapy. Theranostics 8:2992–3006

Jadvar H, Chen X, Cai W, Mahmood U (2018) Radiotheranostics in cancer diagnosis and management. Radiology 286:388–400

Jia L, Li X, Cheng D, Zhang L (2019) Fluorine-18 click radiosynthesis and microPET/CT evaluation of a small peptide-a potential PET probe for carbonic anhydrase IX. Bioorg Med Chem 27:785–789

Kaluz S, Kaluzová M, Liao SY, Lerman M, Stanbridge EJ (2009) Transcriptional control of the tumor- and hypoxia-marker carbonic anhydrase 9: a one transcription factor (HIF-1) show? Biochim Biophys Acta Rev Cancer 1795:162–172

Kozempel J, Mokhodoeva O, Vlk M (2018) Progress in targeted alpha-particle therapy. What we learned about recoils release from in vivo generators. Molecules 23

Krall N, Pretto F, Mattarella M, Muller C, Neri D (2016) A 99mTc-labeled ligand of carbonic anhydrase IX selectively targets renal cell carcinoma in vivo. J Nucl Med 57:943–949

Lau J, Pan J, Zhang Z, Hundal-Jabal N, Liu Z, Bénard F, Lin KS (2014) Synthesis and evaluation of 18 F-labeled tertiary benzenesulfonamides for imaging carbonic anhydrase IX expression in tumours with positron emission tomography. Bioorganic Med Chem Lett 24:3064–3068

Lau J, Liu Z, Lin K-S, Pan J, Zhang Z, Vullo D, Supuran CT, Perrin DM, Bénard F (2015) Trimeric radiofluorinated sulfonamide derivatives to achieve in vivo selectivity for carbonic anhydrase IX-targeted PET imaging. J Nucl Med 56:1434–1440

Lau J, Zhang Z, Jenni S, Kuo HT, Liu Z, Vullo D, Supuran CT, Lin KS, Bénard F (2016) PET imaging of carbonic anhydrase IX expression of HT-29 tumor xenograft mice with 68Ga-labeled benzenesulfonamides. Mol Pharm 13:1137–1146

Lau J, Lin KS, Bénard F (2017) Past, present, and future: development of theranostic agents targeting carbonic anhydrase IX. Theranostics 7:4322–4339

Li Z, Bao S, Wu Q, Wang H, Eyler C, Sathornsumetee S, Shi Q, Cao Y, Lathia J, McLendon RE, Hjelmeland AB, Rich JN (2009) Hypoxia-inducible factors regulate tumorigenic capacity of glioma stem cells. Cancer Cell 15:501–513

Li J, Zhang G, Wang X, Li X-F (2015) Is carbonic anhydrase IX a validated target for molecular imaging of cancer and hypoxia? Futur Oncol 11:1531–1541

Lopci E, Grassi I, Chiti A, Nanni C, Cicoria G, Toschi L, Fonti C, Lodi F, Mattioli S, Fanti S (2014) PET radiopharmaceuticals for imaging of tumor hypoxia: a review of the evidence. Am J Nucl Med Mol Imaging 4:365–384

Lou Y, McDonald PC, Oloumi A, Chia S, Ostlund C, Ahmadi A, Kyle A, Auf Dem Keller U, Leung S, Huntsman D, Clarke B, Sutherland BW, Waterhouse D, Bally M, Roskelley C, Overall CM, Minchinton A, Pacchiano F, Carta F, Scozzafava A, Touisni N, Winum JY, Supuran CT, Dedhar S (2011) Targeting tumor hypoxia: suppression of breast tumor growth and metastasis by novel carbonic anhydrase IX inhibitors. Cancer Res 71:3364–3376

McDonald PC, Winum J-Y, Supuran CT, Dedhar S, McDonald PC, Winum J-Y, Supuran CT, Dedhar S (2012) Recent developments in targeting carbonic anhydrase IX for cancer therapeutics. Oncotarget 3:84–97

Merkx R, Heskamp S, Mulders P, Rijpkema M, Oosterwijk E, Wheatcroft M, Kip A, Morgenstern A, Bruchertseifer F (2019) 225Ac-labeled girentuximab for targeted alpha therapy of CAIX-expressing renal cell cancer xenografts. J Med Imaging Radiat Sci 50:S25

Minn I, Koo SM, Lee HS, Brummet M, Rowe SP, Gorin MA, Sysa-Shah P, Lewis WD, Ahn H-H, Wang Y, Banerjee SR, Mease RC, Nimmagadda S, Allaf ME, Pomper MG, Yang X (2016) [64Cu]XYIMSR-06: A dual-motif CAIX ligand for PET imaging of clear cell renal cell carcinoma. Oncotarget 7:56471–56479

Moroz E, Carlin S, Dyomina K, Burke S, Thaler HT, Blasberg R, Serganova I (2009) Real-time imaging of HIF-1α stabilization and degradation. PLoS One 4:e5077

Morris MR, Hughes DJ, Tian YM, Ricketts CJ, Lau KW, Gentle D, Shuib S, Serrano-Fernandez P, Lubinski J, Wiesener MS, Pugh CW, Latif F, Ratcliffe PJ, Maher ER (2009) Mutation analysis of hypoxia-inducible factors HIF1A and HIF2A in renal cell carcinoma. Anticancer Res 29:4337–4343

Muselaers CHJ, Boerman OC, Oosterwijk E, Langenhuijsen JF, Oyen WJG, Mulders PFA (2013) Indium-111-labeled girentuximab immunoSPECT as a diagnostic tool in clear cell renal cell carcinoma. Eur Urol 63:1101–1106

Muselaers CHJ, Rijpkema M, Bos DL, Langenhuijsen JF, Oyen WJG, Mulders PFA, Oosterwijk E, Boerman OC (2015) Radionuclide and fluorescence imaging of clear cell renal cell carcinoma using dual labeled anti-carbonic anhydrase IX antibody G250. J Urol 194:532–538

Muselaers CHJ, Boers-Sonderen MJ, Van Oostenbrugge TJ, Boerman OC, Desar IME, Stillebroer AB, Mulder SF, Van Herpen CML, Langenhuijsen JF, Oosterwijk E, Oyen WJG, Mulders PFA (2016) Phase 2 study of lutetium 177-labeled anti-carbonic anhydrase IX monoclonal antibody girentuximab in patients with advanced renal cell carcinoma. Eur Urol 69:767–770

Oosterwdk E, Ruiter DJ, Hoedemaeker PJ, Pauwels EKJ, Jonas U, Zwartendijk I, Warnaar SO (1986) Monoclonal antibody G 250 recognizes a determinant present in renal-cell carcinoma and absent from normal kidney. Int J Cancer 38:489–494

Oosterwijk-Wakka JC, Kats-Ugurlu G, Leenders WPJ, Kiemeney LALM, Old LJ, Mulders PFA, Oosterwijk E (2011) Effect of tyrosine kinase inhibitor treatment of renal cell carcinoma on the accumulation of carbonic anhydrase IX-specific chimeric monoclonal antibody cG250. BJU Int 107:118–125

Oosterwijk-Wakka JC, Boerman OC, Mulders PFAM, Oosterwijk E (2013) Application of monoclonal antibody G250 recognizing carbonic anhydrase IX in renal cell carcinoma. Int J Mol Sci 14:11402–11423

Oosterwijk E, Bander NH, Divgi CR, Welt S, Wakka JC, Finn RD, Carswell EA, Larson SM, Warnaar SO, Fleuren GJ, Oettgen HF, Old LJ (1993) Antibody localization in human renal cell carcinoma: a phase I study of monoclonal antibody G250. J Clin Oncol 11:738–750

Parks SK, Chiche J, Pouyssegur J (2011) pH control mechanisms of tumor survival and growth. J Cell Physiol 226:299–308

Pastorekova S, Ratcliffe PJ, Pastorek J (2008) Molecular mechanisms of carbonic anhydrase IX-mediated pH regulation under hypoxia. BJU Int 101:8–15

Peeters SGJA, Dubois L, Lieuwes NG, Laan D, Mooijer M, Schuit RC, Vullo D, Supuran CT, Eriksson J, Windhorst AD, Lambin P (2015) [18F]VM4-037 MicroPET imaging and biodistribution of two in vivo CAIX-expressing tumor models. Mol Imaging Biol 17:615–619

Rafajová M, Zatovicová M, Kettmann R, Pastorek J, Pastoreková S (2004) Induction by hypoxia combined with low glucose or low bicarbonate and high posttranslational stability upon reoxygenation contribute to carbonic anhydrase IX expression in cancer cells. Int J Oncol 24:995–1004

Rajendran JG, Krohn KA (2015) F-18 fluoromisonidazole for imaging tumor hypoxia: imaging the microenvironment for personalized cancer therapy. Semin Nucl Med 45:151–162

Rajendran JG, Wilson DC, Conrad EU, Peterson LM, Bruckner JD, Rasey JS, Chin LK, Hofstrand PD, Grierson JR, Eary JF, Krohn KA (2003) [18F]FMISO and [18F]FDG PET imaging in soft tissue sarcomas: Correlation of hypoxia, metabolism and VEGF expression. Eur J Nucl Med Mol Imaging 30:695–704

Rami M, Cecchi A, Montero JL, Innocenti A, Vullo D, Scozzafava A, Winum JY, Supuran CT (2008) Carbonic anhydrase inhibitors: design of membrane-impermeant copper(II) complexes of DTPA-, DOTA-, and TETA-tailed sulfonamides targeting the tumor-associated transmembrane isoform IX. ChemMedChem 3:1780–1788

Rana S, Nissen F, Marr A, Markert A, Altmann A, Mier W, Debus J, Haberkorn U, Askoxylakis V (2012) Optimization of a novel peptide ligand targeting human carbonic anhydrase IX. PLoS One 7:e38279

Rana S, Nissen F, Lindner T, Altmann A, Mier W, Debus J, Haberkorn U (2013) Askoxylakis V (2013) Screening of a novel peptide targeting the proteoglycan-Like region of human carbonic anhydrase 9. Mol Imaging 12(7290):00066

Rault E, Vandenberghe S, Van Holen R, De Beenhouwer J, Staelens S, Lemahieu I (2007) Comparison of image quality of different iodine isotopes (I-123, I-124, and I-131). Cancer Biother Radiopharm 22:423–430

Ridge CA, Pua BB, Madoff DC (2014) Epidemiology and staging of renal cell carcinoma. Semin Intervent Radiol 31:3–8

Scott AM, Wolchok JD, Old LJ (2012) Antibody therapy of cancer. Nat Rev Cancer 12:278–287

Sharkey RM, Goldenberg DM (2009) Targeted therapy of cancer: new prospects for antibodies and immunoconjugates. CA Cancer J Clin 56:226–243

Sneddon D, Niemans R, Bauwens M, Yaromina A, Van Kuijk SJA, Lieuwes NG, Biemans R, Pooters I, Pellegrini PA, Lengkeek NA, Greguric I, Tonissen KF, Supuran CT, Lambin P, Dubois L, Poulsen SA (2016) Synthesis and in vivo biological evaluation of 68Ga-labeled carbonic anhydrase IX targeting small molecules for positron emission tomography. J Med Chem 59:6431–6443

Steffens MG, Boerman OC, de Mulder PH, Oyen WJ, Buijs WC, Witjes JA, van den Broek WJ, Oosterwijk-Wakka JC, Debruyne FM, Corstens FH, Oosterwijk E (1999) Phase I radioimmunotherapy of metastatic renal cell carcinoma with 131I-labeled chimeric monoclonal antibody G250. Clin Cancer Res 5:3268s–3274s

Stillebroer AB, Boerman OC, Desar IME, Boers-Sonderen MJ, Van Herpen CML, Langenhuijsen JF, Smith-Jones PM, Oosterwijk E, Oyen WJG, Mulders PFA (2013) Phase 1 radioimmunotherapy study with lutetium 177-labeled anti-carbonic anhydrase ix monoclonal antibody girentuximab in patients with advanced renal cell carcinoma. Eur Urol 64:478–485

Supuran CT (2008) Carbonic anhydrases: novel therapeutic applications for inhibitors and activators. Nat Rev Drug Discov 7:168–181

Supuran CT (2017) Carbonic anhydrase inhibition and the management of hypoxic tumors. Metabolites 7:48

Supuran CT, Briganti F, Tilli S, Chegwidden WR, Scozzafava A (2001) Carbonic anhydrase inhibitors: sulfonamides as antitumor agents? Bioorganic Med Chem 9:703–714

Turkbey B, Lindenberg ML, Adler S, Kurdziel KA, McKinney YL, Weaver J, Vocke CD, Anver M, Bratslavsky G, Eclarinal P, Kwarteng G, Lin FI, Yaqub-Ogun N, Merino MJ, Marston Linehan W, Choyke PL, Metwalli AR (2016) PET/CT imaging of renal cell carcinoma with 18F-VM4-037: a phase II pilot study. Abdom Radiol 41:109–118

Walsh JC, Lebedev A, Aten E, Madsen K, Marciano L, Kolb HC (2014) The clinical importance of assessing tumor hypoxia: relationship of tumor hypoxia to prognosis and therapeutic opportunities. Antioxid Redox Signal 21:1516–1554

Weissleder R, Mahmood U (2001) Molecular imaging. Radiology 219:316–333

Wichert M, Krall N, Decurtins W, Franzini RM, Pretto F, Schneider P, Neri D, Scheuermann J (2015) Dual-display of small molecules enables the discovery of ligand pairs and facilitates affinity maturation. Nat Chem 7:241–249

Wilson WR, Hay MP (2011) Targeting hypoxia in cancer therapy. Nat Rev Cancer 11:393–410

Wykoff CC, Beasley NJP, Watson PH, Turner KJ, Pastorek J, Sibtain A, Wilson GD, Turley H, Talks KL, Maxwell PH, Pugh CW, Ratcliffe PJ, Harris AL (2000) Hypoxia-inducible expression of tumor-associated carbonic anhydrases. Cancer Res 60:7075–7083

Yang X, Minn I, Rowe SP, Banerjee SR, Gorin MA, Brummet M, Lee HS, Koo SM, Sysa-Shah P, Mease RC, Nimmagadda S, Allaf ME, Pomper MG (2015) Imaging of carbonic anhydrase IX with an 111In-labeled dual-motif inhibitor. Oncotarget 6:33733–33742

Yang X, Zhu H, Yang X, Li N, Huang H, Liu T, Guo X, Xu X, Xia L, Deng C, Tian X, Yang Z (2019) Targeting CAIX with [64Cu]XYIMSR-06 small molecular radiotracer enables noninvasive PET imaging of malignant glioma in U87 MG tumor cell xenograft mice. Mol Pharm 16:1532–1540

Zhang J, Zhang Q (2018) VHL and hypoxia signaling: beyond HIF in cancer. Biomedicines 6:35

Zhang Z, Lau J, Zhang C, Colpo N, Nocentini A, Supuran CT, Bénard F, Lin KS (2017) Design, synthesis and evaluation of 18 F-labeled cationic carbonic anhydrase IX inhibitors for PET imaging. J Enzyme Inhib Med Chem 32:722–730